COMPLEMENTARY MODELS FOR PREDICTING THE FORMATION RESISTIVITY FACTOR AND RESISTIVITY INDEX AT OVERBURDEN CONDITIONS

Meysam Nourani[*], *Stefano Pruno, Mohammad Ghasemi, Muhamet Meti Fazlija, Byron Gonzalez, Jone Bråstein and Hans-Erik Rodvelt*

Stratum Reservoir AS, Stavanger, Norway

Abstract. In this study, new analytical approaches are presented to predict Formation Resistivity Factor (FRF) and Resistivity Index (RI) under overburden pressure conditions. The new models are extensions of the recently presented by Nourani et al. and developed based on Rock Resistivity Modulus (RRM), True Resistivity Modulus (TRM) and Archie's equations. The major criticism of lately presented models is that for the sake of simplicity in deriving the equations, the authors supposed cementation factor and saturation exponent are independent of the overburden pressure. To address this limitation, the present study based on experimental data assumes linear relationships between cementation factor and overburden pressure, and between saturation exponent and overburden pressure. To estimate FRF and RI, these models need the gradients of the linear functions which are calculated based on the overburden resistivity data. The developed models are compared to the previous model and reasonable agreements were obtained. The new models are more complex in formulation and application, whereas the simpler FRF model presented in the previous study is more practical and good enough for predicting FRF at overburden pressures, especially when FRF has been measured only at ambient condition.

Introduction

Archie's Formation Resistivity Factor (FRF) and Resistivity Index (RI) are essential petrophysical properties for log calibration and reservoir characterisation [1]. Archie's empirical equations describe electrical properties of sandstones. They have been derived based on the assumption that the rock is clean, clay-free and strongly water-wet. Additionally, it is assumed that the pore geometry is simple and unimodal, the rock grains are non-conductive, and all the water contributes to electrical current flow [2–4].

The estimation of the volume of hydrocarbon initially in place (HCIIP) at reservoir conditions is a vital component of reservoir management. This volume is determined by the water saturation, porosity, and the total volume of the reservoir. To obtain this information, the water saturation and porosity of the reservoir must first be determined. Once these values are estimated, then the HCIIP can be calculated by multiplying the water saturation, porosity, and total reservoir volume [5,6].

It is necessary to calibrate electrical logs in order to calculate the saturation of water by applying Archie's equation cementation m-exponent and saturation n-exponent. In order to accurately determine these exponents, laboratory measurements on core samples must be performed. To ensure reliable results, the empirical parameters must be quantified at representative reservoir overburden pressure and temperature conditions. The most effective way to do this is to use the results from Special Core Analysis (SCAL) measurements. With SCAL, Archie's exponents can be accurately determined in the laboratory, and the water saturation is calculated by using the Archie's equations. FRF and RI SCAL laboratory experiments are designed to simulate reservoir conditions as accurately as possible, but usually they are conducted at lower overburden pressure and temperature conditions. Due to limited time, complexity of measurements, and higher expenses, it is common to perform FRF experiments at a single overburden pressure in order to keep expenses within budget [7]. Thus, testing conditions are usually dissimilar to the actual conditions in the reservoir. Despite the fact that the results can be dissimilar and are not totally representative, they can still be of value for petrophysical interpretations. Therefore, it is important to consider the limitations of the testing conditions when analysing the results of FRF tests.

Overburden pressure is a critical concept in geology as it defines the stress or hydrostatic pressure that is exerted by the overlying layers of material (rock, salt, water) on a reference point or layer. The total pressure increases as more material is added above the reference point. The formation then compresses once the overburden pressure surpasses the limit of the pore pressure in the permeable rock[8]. As a result of compaction, the tortuosity of flow paths is altered significantly, with the pore sizes becoming smaller. This, in turn, causes the porosity of the material to decrease. According to Archie's law, as porosity decreases, the FRF increases [9–12]. Numerous researchers have conducted studies on the effect of confining pressure on the FRF of various rock samples. The results of these studies have been compelling, showing that the FRF increases as the confining stress and overburden pressure increase [9–20]. The effect of

[*] Corresponding author: meysam.nourani@stratumreservoir.com

overburden pressure on FRF is highly dependent on the type of rock, as well as its lithology, pore size distribution, clays content, fluid saturation, porosity, and permeability. Studies have found that different rocks exhibit varied responses to overburden pressure due to these parameters [21].

Recently, Nourani et al. [22] has developed mathematical models based on Archie's equation for predicting FRF and RI under different overburden pressures. FRF models are referred to both, the Multi-FRF model and the Single-FRF model. The Multi-FRF model expresses the relationship between the rock resistivity modulus (RRM, γ_{R_o}[bar^{-1}]), confining pressure difference (ΔP[bar]) and the reference *FRF* as follows:

$$FRF_2 = FRF_1 \, e^{-\gamma_{R_o} \Delta P} \tag{1}$$

The Single-FRF model relates the cementation exponent (m), the pore volume compressibility (C_p[bar^{-1}]), bulk compressibility (C_b[bar^{-1}]) and the reference *FRF* as:

$$FRF_2 = FRF_1 \, e^{m\,(C_p - C_b)\Delta P} \tag{2}$$

The RI model is dependent on the cementation saturation exponent (n), C_p, the formation brine compressibility (C_{fb}[bar^{-1}]) and the reference *RI* as:

$$RI_2 = RI_1 \, e^{n(C_{fb} - C_p)\Delta P} \tag{3}$$

The models, however, have been met with some criticism due to the authors' simplified assumption that the cementation and saturation exponents are independent of the overburden pressure. This analytical-experimental study seeks to explore the relationship between FRF, RI, and overburden pressure. Through this work, the aim is to develop complementary mathematical models which enable prediction of FRF and RI under different overburden pressures, with the understanding that saturation and cementation exponents are linear functions of increasing overburden pressure.

Development of the FRF Models

FRF is defined as the ratio of the resistivity of completely saturated rock with brine (R_o [Ωm]) to the resistivity of formation water (R_w [Ωm]). The FRF is related to the porosity (φ [fraction]) and cementation exponent by the Archie equation:

$$FRF = \frac{R_o}{R_w} = \varphi^{-m} \tag{4}$$

Porosity is a measure of the amount of space within a material that is filled with voids or pores. It is typically expressed as a ratio of the pore space volume (V_p) to the bulk volume (V_b) of the rock. The Resistivity Index (RI) is the second essential dimensionless parameter that is calculated as the ratio of the resistivity of the rock when partially saturated with water (R_t [Ω m]) to the resistivity of the rock when it is fully saturated with water (R_o). This parameter is related to the amount of water present in the pore space and is an important factor when calculating the electrical properties of the rock. It is related to the water saturation (S_w [fraction]), as follows [1]:

$$RI = \frac{R_t}{R_o} = S_w^{-n} \tag{5}$$

RRM is the measure of the relative change in the rock resistivity of rock fully saturated with brine in response to a pressure change as follows [22]:

$$\gamma_{R_o} = -\frac{1}{R_o}\frac{\partial R_o}{\partial P} \tag{6}$$

Similarly, the water resistivity modulus (WRM) and the true resistivity modulus (TRM) are defined as:

$$\gamma_{R_w} = -\frac{1}{R_w}\frac{\partial R_w}{\partial P} \tag{7}$$

$$\gamma_{R_t} = -\frac{1}{R_t}\frac{\partial R_t}{\partial P} \tag{8}$$

By combining Equations (4) and (6), RMM can be calculated using the following equation:

$$\gamma_{R_o} = -\frac{\varphi^m}{R_w}\frac{\partial\left(\frac{R_w}{\varphi^m}\right)}{\partial P} \tag{9}$$

Figures 1 and 2 are shown some examples of linear relationships between cementation exponent and overburden pressure for sandstone and carbonate samples, respectively.

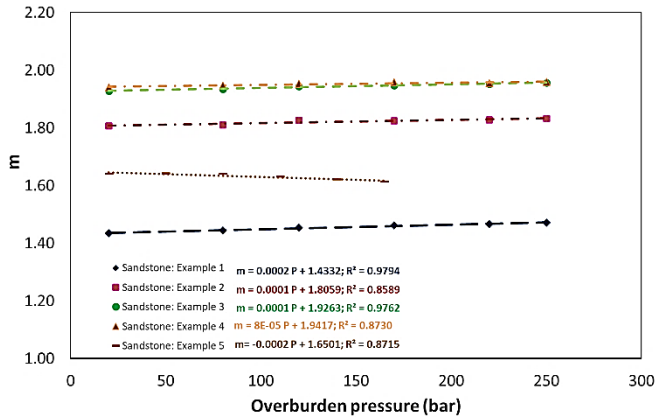

Fig. 1. Examples of linear relationships between cementation exponent and overburden pressure for sandstone samples.

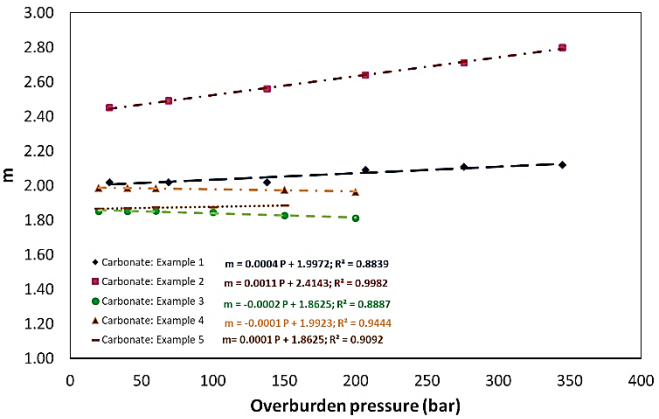

Fig. 2. Examples of linear relationships between cementation exponent and overburden pressure for carbonate samples.

In light of experimental observations, it was assumed that the cementation exponent was linearly related to overburden pressure as follows:

$$m = a_1 P + b_1 \quad (10)$$

where a_1 and b_1 are the slope and the intercept of the drawn line between overburden pressure and cementation exponent, respectively. Consequently, by assuming a linearity between cementation exponent and overburden pressure over the pressure interval of interest, taking the derivative of the term $(\frac{R_w}{\varphi^m})$ with respect to pressure in Equation (9) and rearranging it, yields the following equation:

$$\gamma_{R_o} = -\frac{1}{R_w}\frac{\partial R_w}{\partial P} + a_1 Ln\varphi + \frac{m}{\varphi}\frac{\partial \varphi}{\partial P} \quad (11)$$

The derivative of the porosity with respect to pressure can be expressed by the following equation [22]:

$$\frac{\partial \varphi}{\partial P} = \varphi\,(C_b - C_p) \quad (12)$$

By separating the φ in Equation (12) and integrating while assuming constant $(C_b - C_p)$ over the pressure interval of interest, the Ln φ at a given overburden pressure can be calculated as follows:

$$Ln\,\varphi = Ln\,\varphi_1 + (C_b - C_p)(P - P_1) \quad (13)$$

where φ_1 and P_1 are porosity and pressure at ambient condition, respectively. By combining Equations (7), (10), (11), (12) and (13), yields the following equation:

$$\gamma_{R_o} = \gamma_{R_w} + (2a_1 P - a_1 P_1 + b_1)(C_b - C_p) + a_1 Ln\varphi_1 \quad (14)$$

Considering that the water resistivity does not vary with pressure, the WRM over the pressure interval is zero [22]. In Equation (6), separating the R_o and integrating with respect to the pressure interval of interest while calculating RRM by Equation (14), the R_o at a given overburden pressure can be determined as follows:

$$R_{o_2} = R_{o_1} e^{[m_2(C_p - C_b) - a_1 Ln\varphi_1]\Delta P} \quad (15)$$

where R_{o_1} is rock resistivity at initial pressure. As a result of dividing both sides of Equation (15) by the water resistivity, the overburden FRF is determined as:

$$FRF_2 = FRF_1\, e^{[m_2(C_p - C_b) - a_1 Ln\varphi_1]\Delta P} \quad (16)$$

Validating the Complementary FRF Model

The developed Complementary FRF model was applied and validated using the same data set from five North Sea reservoirs as Nourani et al. The dataset involves resistivity data of fifty-five (55) 1.5-inch diameter plugs from five different North Sea reservoirs. The range of porosity, permeability, grain density and bulk mineral composition of the samples have been previously presented [22]. Nourani et al. previously showed an example where Single-FRF model had the largest deviation from experimental data (Figure 3). To investigate the accuracy of the Complementary FRF model, the same example data is used.

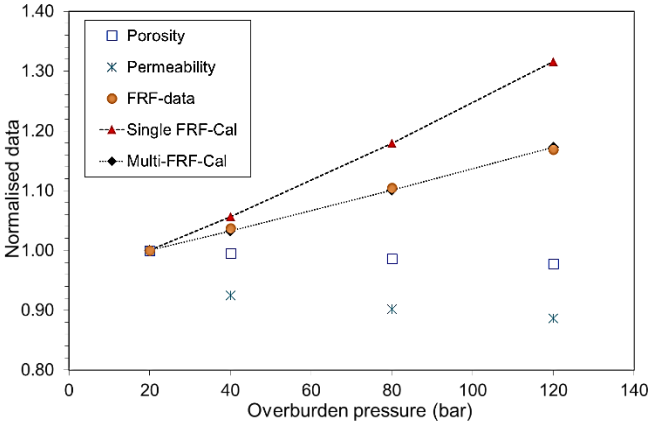

Fig. 3. Example, fitting of Multi-FRF model and Single-FRF model to FRF data; relationship between the overburden pressure and normalized porosity, permeability and FRF [22].

In Figure 4, the overburden pressure and cementation exponent data from the example are very well fitted linearly.

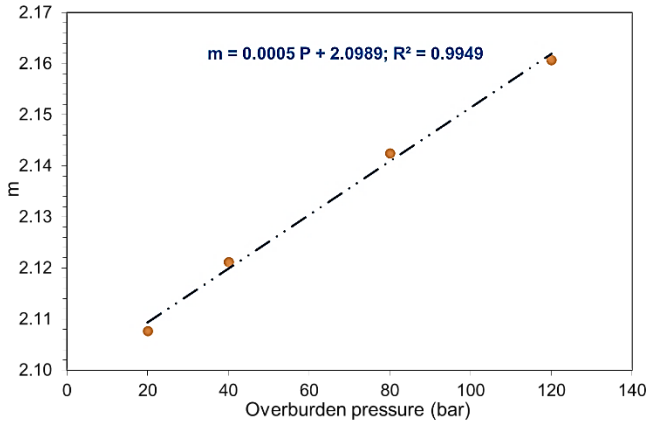

Fig. 4. Linear fitting to overburden pressure and cementation exponent data from the example in figure (3).

Equation (16) was fitted to the measured FRF data using the slope and the intercept of the line on Figure 4. Figure 5 shows an excellent agreement between the Complementary FRF model and the measured data (R^2=0.9999).

In Figure 6, the modelled overburden FRF estimated using the Complementary FRF model is compared to the measured overburden FRF of the fifty-five (55) core plug samples collected from five North Sea reservoirs. The model-predicted overburden FRF closely matches the experimental laboratory data. This demonstrates remarkable accuracy in the Complementary FRF model prediction and indicates that the model is highly reliable and effective. Table 1 presents the R^2 values calculated by Single-FRF, Multi-FRF and Complementary FRF models for North Sea reservoirs. It is observed that the Complementary FRF model shows a higher degree of accuracy than the Single-FRF and the Multi-FRF models. The R^2 values for the Complementary FRF model are higher than those of the other two models, indicating the superior accuracy of the Complementary-FRF model. This is expected, since the Complementary FRF model has the

capability of considering multiple factors, thus providing a more accurate prediction. The Single-FRF and the Multi-FRF models, on the other hand, are limited by the factors considered.

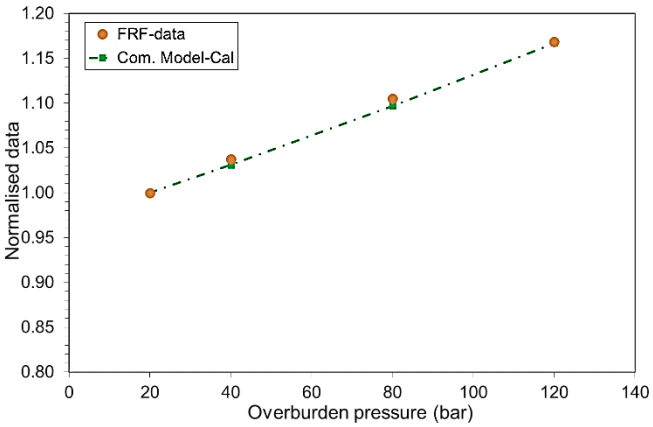

Fig. 5. Example, fitting of the Complementary FRF model to FRF data. The fitting shows excellent agreement with the experimental data ($R^2 = 0.9999$).

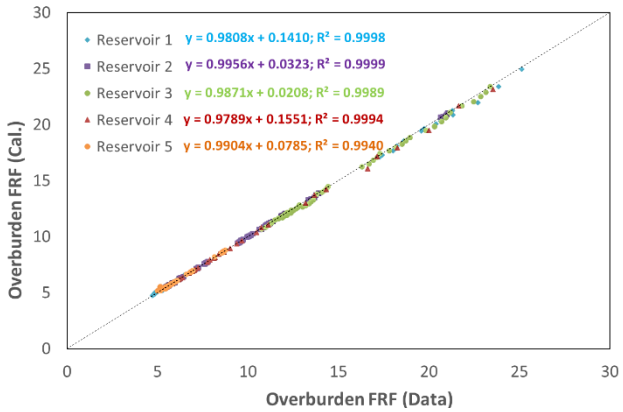

Fig. 6. Overburden FRF calculated using the Complementary FRF model, Equation (16), versus measured overburden FRF for five North Sea reservoirs.

Table 1. Overview of the corresponding R^2 from FRF models.

Res.	R^2 (Single-FRF)	R^2(Multi-FRF)	R^2(Comp.-FRF)
1	0.9961	0.9994	0.9998
2	0.9996	0.9984	0.9999
3	0.9949	0.9987	0.9989
4	0.9968	0.9992	0.9994
5	0.9767	0.9908	0.9940

Development of the Complementary RI Model

The calculation of RI can be carried out using a similar modelling approach. Following experimental observations [20], it was assumed that the saturation exponent was linearly related to overburden pressure as:

$$n = a_2 P + b_2 \tag{17}$$

where a_2 and b_2 are the slope and the intercept of the drawn line between overburden pressure and saturation exponent, respectively. The following equation can be obtained by combining Equations (4), (5), and (8):

$$\gamma_{R_t} = -\frac{\varphi^m S_w{}^n}{R_w} \times \frac{\partial(\frac{R_w}{\varphi^m S_w{}^n})}{\partial P} \tag{18}$$

Hence, by assuming a linear relationship between saturation exponent and overburden pressure over the pressure interval of interest, and taking the derivative of the term $(\frac{R_w}{\varphi^m S_w{}^n})$ with respect to pressure in Equation (18) and rearranging it, the TRM can be calculated as follows:

$$\gamma_{R_t} = \frac{-1}{R_w}\frac{\partial R_w}{\partial P} + a_1\, Ln\varphi + \frac{m}{\varphi}\frac{\partial \varphi}{\partial P} + a_2\, LnS_w + \frac{n}{S_w}\frac{\partial S_w}{\partial P} \tag{19}$$

The formation brine compressibility; C_{fb}, is expressed as [23]:

$$C_{fb} = -\frac{1}{V_w}\frac{\partial V_w}{\partial P} \tag{20}$$

The derivative of the S_w with respect to pressure can be calculated by the following equation [22]:

$$\frac{\partial S_w}{\partial P} = S_w(\, C_p - C_{fb}) \tag{21}$$

By separating the S_w in Equation (21) and integrating while assuming constant $(C_b - C_{fb})$ over the pressure interval of interest, the Ln S_w at a given overburden pressure can be calculated as follows:

$$Ln\, S_w = Ln\, S_{w_1} + (C_b - C_{fb})(P - P_1) \tag{22}$$

Thus, the TRM can be calculated by replacing Equations (7), (12), (13), (21) and (22) into Equation (19) as below:

$$\begin{aligned}\gamma_{R_t} &= 2P\left[a_1(C_b - C_p) + a_2(C_b - C_{fb})\right] \\ &- P_1\left[a_1(C_b - C_p) + a_2(C_b - C_{fb})\right] \\ &+ b_1(C_b - C_p) + b_2(C_b - C_{fb}) + a_1 Ln\varphi_1 + a_2\, LnS_{w_1}\end{aligned} \tag{23}$$

In Equation (8), separating the R_t and integrating while calculating TRM by Equation (23) with respect to the pressure interval of interest, the R_t at a given overburden pressure can be determined as follows:

$$R_{t_2} = R_{t_1} e^{[m_2(C_p - C_b) + n_2(C_{fb} - C_p) - a_1 Ln\varphi_1 - a_2\, LnS_{w_1}]\Delta P} \tag{24}$$

By dividing Equation (24) by Equation (15), the RI at a given overburden pressure can be estimated as:

$$RI_2 = RI_1\, e^{[n_2(C_{fb} - C_p) - a_2\, LnS_{w_1}]\Delta P} \tag{25}$$

Results and Discussion

The Complementary FRF model, Equation (16), converts to the Single-FRF model, Equation (2), if the slope of the line

between overburden pressure and cementation exponent, a_1 coefficient, approaches zero. A similar result can be obtained if the slope of the line between the overburden pressure and saturation exponent in Equation (17), a_2 coefficient, approaches zero, then Equation (25), the Complementary RI model, converts to the RI model presented in the previous study.

Table 2 summarizes a comparison of the performance and data requirements of the developed FRF models. It is essential that the data on FRF and porosity are available at ambient conditions in order to run the Single-FRF model. The ambient porosity can be used to estimate the necessary compressibilities based on correlations available in the literature [22]. In order to achieve a satisfactory match between the Single-FRF model and the experimental data, porosity must have been measured at least at two additional overburden pressures. Consequently, it is possible to determine the difference between pore and bulk compressibilities by knowing at least three overburden porosities. For the Multi-FRF model to be run, FRF data must be available at two overburden pressures. The two FRF data can be used to estimate roughly the required RRM. Ideally, to obtain an accurate and satisfactory match between the Multi-FRF model and the experimental data, FRF needs to be measured at least at one more overburden pressure. For the Complementary FRF model to operate, FRF and porosity data must be available at two overburden pressures. It is possible to estimate approximately the a1 and $(C_b - C_p)$ using the two FRF and porosity data. Nevertheless, at least another measurement of FRF and porosity at overburden pressure should be conducted in order to provide a suitable match between the Complementary FRF model and the experimental results.

Table 2. Comparison of the performance and data requirements of the developed FRF models.

FRF Model	Min. data required to run the model	Min. data required for a successful match	Average Rel. Er. (%)
Single	FRF_1 φ_1	FRF_1 $\varphi_1, \varphi_2 and\ \varphi_3$	5
Multi	FRF_1 and FRF_2	$FRF_1, FRF_2\ and\ FRF_3$	2-3
Comp.	FRF_1 and FRF_2 φ_1 and φ_2	$FRF_1, FRF_2\ and\ FRF_3$ $\varphi_1, \varphi_2\ and\ \varphi_3$	< 1

As can be seen in Figure 3, the Single-FRF model deviates the most from the measured FRF data at 120 bar overburden pressure. Whereas only 0.4% and 0.2% deviations from the measured FRF data were observed for the predictions of Multi-FRF model and the Complementary FRF model, respectively.

The average relative error for predicting overburden FRF for samples from North Sea reservoirs by using the Complementary FRF model is less than 1%, while it was reported around 5% by using the Single-FRF model in previous study. Although Table 1 shows improvements in accuracy using the Complementary FRF model, the R^2 values for the Multi-FRF model are very close to those applied the Complementary FRF model. Aside from this, the single-FRF model still has acceptable and valuable R^2 values. The Multi-FRF model is derived on the premise that the cementation exponent does not vary with the overburden pressure. However, the results of the FRF predictions are very close to those of the Complementary FRF model since this model actually considers an average RRM over the pressure intervals of interest and as cementation factor variation with overburden pressure is in some cases insignificant, the FRF prediction results are very similar to the Complementary FRF model predictions.

Conclusions

In this study, complementary analytical FRF and RI models have been developed. To do this, assumptions were made that saturation and cementation exponents will behave linearly in relation to increasing overburden pressure.

The Complementary FRF Model includes the cementation exponent at overburden pressure, the pore volume compressibility, the bulk compressibility, the ambient porosity, and the slope of the line between overburden pressure and cementation exponent. Components of the Complementary RI Model include the saturation exponent at overburden pressure, the formation brine compressibility, the pore volume compressibility, the ambient water saturation, and the slope of the line between overburden pressure and saturation exponent.

The accuracy of the Complementary FRF model and the Multi-FRF model are higher than the accuracy of the Single-FRF model. Both the Complementary FRF and the Multi-FRF models have almost the same accuracy, though the complementary model is slightly better. The Complementary FRF model, on the other hand, is more complex than the Single-FRF and Multi-FRF models, therefore it requires a greater volume of data for it to be functional, compared to the Single-FRF and Multi-FRF models. In order to obtain the parameters required for both the Complementary FRF and Multi-FRF models, FRF must be already measured under several overburden pressures. Hence, these two models can interpolate and extrapolate FRF data to any overburden pressure, within the boundary conditions of Archie's equations. Despite the slightly inferior accuracy of the Single-FRF model as compared with both the Complementary FRF and the Multi-FRF models, it is still a viable solution when it comes to predicting the FRF at overburden pressure, especially when experimental overburden FRF data are not available.

Nomenclature

a_1 Slope of the line in Equation (10), bar^{-1}
b_1 Intercept of the line in Equation (10), dimensionless
a_2 Slope of the line in Equation (17), bar^{-1}
b_2 Intercept of the line in Equation (17), dimensionless
C_b Bulk compressibility, bar^{-1}
C_{fb} Formation brine compressibility, bar^{-1}
C_p Pore volume compressibility, bar^{-1}
ΔP Confining pressure difference, bar
φ Porosity, fraction
FRF Formation Resistivity Factor, dimensionless

γ_{C_o} Rock conductivity modulus, bar^{-1}
γ_{R_o} Rock resistivity modulus, bar^{-1}
γ_{R_t} True resistivity modulus, bar^{-1}
γ_{R_w} Water resistivity modulus, bar^{-1}
$HCIIP$ Volume of hydrocarbon initially in place at reservoir conditions, m^3
m Cementation factor, dimensionless
n Saturation exponent, dimensionless
P Pressure, bar
RI Resistivity Index, dimensionless
R_o Resistivity of rock fully saturated with brine, Ωm
R_t Resistivity of rock partially saturated with brine, Ωm
R_w Formation water resistivity, Ωm
S_w Water saturation, fraction
V Volume of the reservoir, m^3
V_b Bulk volume, m^3
V_p Pore space volume, m^3
V_w Volume of the formation brine, m^3

References

[1] Archie, G. E., 1942, The electrical resistivity log as an aid in determining some reservoir characteristics: Transactions of the AIME, v. 146, no. 01, p. 54–62, https://doi.org/10.2118/942054-G

[2] Carter, S. L., and H. H. Power, 1962, The relationship between electrical resistivity and brine saturation in reservoir rocks: The Log Analyst, v. 2, no. 05.

[3] Mungan, N., and E. J. Moore, 1968, Certain wettability effects on electrical resistivity in porous media: Journal of Canadian Petroleum Technology, v. 7, no. 01, p. 20–25, https://doi.org/10.2118/68-01-04

[4] Torsæter, O., and M. Abtahi, 2003, Experimental reservoir engineering laboratory workbook: Norwegian University of Science and Technology.

[5] Fleury, M., M. Efnik, and M. Z. Kalam, 2004, Evaluation of water saturation from resistivity in a carbonate field. From laboratory to logs, in Proceedings of International Symposium of the Society of Core Analysts, Abu Dhabi, UAE: p. 5–9.

[6] Masoudi, P., A. Zahedi, M. Ali, A. Farshid, and Z. Seyed Mohammad, 2011, Estimation of in place hydrocarbon volume in multilayered reservoirs using deterministic and probabilistic approaches: Energy exploration & exploitation, v. 29, no. 5, p. 543–557.

[7] McPhee, C., J. Reed, and I. Zubizarreta, 2015, Core analysis: a best practice guide: Elsevier, ISBN:978-0-444-63533-4.

[8] Baker, R. O., H. W. Yarranton, and J. Jensen, 2015, Practical reservoir engineering and characterization: Gulf Professional Publishing, ISBN:978-0-12-801811-8.

[9] Fatt, I., 1957, Effect of overburden and reservoir pressure on electric logging formation factor: AAPG Bulletin, v. 41, no. 11, p. 2456–2466, https://doi.org/10.1306/0BDA59A8-16BD-11D7-8645000102C1865D

[10] Brace, W. F., A. S. Orange, and T. R. Madden, 1965, The effect of pressure on the electrical resistivity of water-saturated crystalline rocks: Journal of Geophysical research, v. 70, no. 22, p. 5669–5678, https://doi.org/10.1029/JZ070i022p05669

[11] Timur, A., W. B. Hempkins, and A. E. Worthington, 1972, Porosity and pressure dependence of formation resistivity factor for sandstones, in Trans CWLS 4th Formation Evaluation Symp.

[12] Jing, X. D., J. S. Archer, and T. S. Daltaban, 1992, Laboratory study of the electrical and hydraulic properties of rocks under simulated reservoir conditions: Marine and Petroleum Geology, v. 9, no. 2, p. 115–127, https://doi.org/10.1016/0264-8172(92)90084-R

[13] Longeron, D. G., M. J. Argaud, and J. P. Feraud, 1986, Effect of overburden pressure, nature, and microscopic distribution of the fluids on electrical properties of rock samples, SPE Paper 15383, in 61st Annual Technical Conference, Society of Petroleum Engineers, New Orleans, LA, October: p. 5–8.

[14] Hashmy, K. H., and J. M. Campbell, 1966, The effect of pore configuration, pressure and temperature on rock resistivity, in SPWLA 7th Annual Logging Symposium: OnePetro.

[15] Wyble, D. O., 1958, Effect of applied pressure on the conductivity, porosity and permeability of sandstones: Journal of Petroleum Technology, v. 10, no. 11, p. 57–59, https://doi.org/10.2118/1081-G

[16] Glanville, C. R., 1959, Laboratory study indicates significant effect of pressure on resistivity of reservoir rock: Journal of Petroleum Technology, v. 11, no. 04, p. 20–26, https://doi.org/10.2118/1153-G

[17] Brace, W. F., and A. S. Orange, 1968, Electrical resistivity changes in saturated rocks during fracture and frictional sliding: Journal of geophysical research, v. 73, no. 4, p. 1433–1445, https://doi.org/10.1029/JB073i004p01433

[18] Parkhomenko, E. I., 1982, Electrical resistivity of minerals and rocks at high temperature and pressure: Reviews of Geophysics, v. 20, no. 2, p. 193–218, https://doi.org/10.1029/RG020i002p00193

[19] Redmond, J. C., 1962, Effect of simulated overburden pressure on the resistivity, porosity and permeability of selected sandstones.: The Pennsylvania State University.

[20] Lewis, M. G., M. M. Sharma, and H. F. Dunlap, 1988, Wettability and stress effects on saturation and cementation exponents, in SPWLA 29th Annual Logging Symposium: OnePetro.

[21] Moore, E. J., S. E. Szasz, and B. F. Whitney, 1966, Determining formation water resistivity from chemical analysis: Journal of Petroleum Technology, v. 18, no. 03, p. 373–376, https://doi.org/10.2118/1337-PA

[22] Nourani M, Pruno S, Ghasemi M, Fazlija MM, Gonzalez B, Rodvelt H-E. Analytical Models for Predicting the Formation Resistivity Factor and Resistivity Index at Overburden Conditions. Petrophysics 2023;64:353–66, https://doi.org/10.30632/PJV64N3-2023a3

[23] Osif, T. L., 1988, The effects of salt, gas, temperature, and pressure on the compressibility of water: SPE reservoir Engineering, v. 3, no. 01, p. 175–181, https://doi.org/10.2118/13174-PA